Laminar Natural Convection in Attics of Rooftops with Depressed Walls

[1]Ola Kamiyo, and [2]Abimbola Dada
[1]Department of Mechanical Engineering, University of Lagos, Lagos, Nigeria
[2]Department of Mechanical Engineering, University of Lagos, Lagos, Nigeria
okamiyo@unilag.edu.ng|olayemi3670@gmail.com|

Received: 09-FEB-2024; Reviewed: 28-JUNE-2024; Accepted: 29-JUNE-2024
https://dx.doi.org/10.4314/fuoyejet.v9i2.15

ORIGINAL RESEARCH

Abstract— Laminar natural convection in the attics of rooftops with depressed upper walls and heated base wall has been investigated numerically using a finite volume CFD package. Selected roofs referred to as Combination, Clerestory and Butterfly roofs are compared with standard isosceles triangular roof having the same pitch and base length. The results obtained show that the depressed wall distorts the multicellular air movement pattern within the attics. It compressed the cells, thereby reducing their sizes and damping their rotation. The depression brings the upper walls closer to the base wall resulting in further breakdown of the convection cells, distortion of the cell shape, modification of the velocity and temperature distribution, higher air pressure and increased heat transfer rate within the area under the depressed walls. Overall, the mean heat transfer rate along the base wall increases with the depth and length of the depressed wall. It is therefore recommended that roof designers should apply caution with depressed walls in order to minimize heat exchange across the ceiling.

Keywords— attic, depressed walls, heat transfer, pitched roofs, natural convection.

1 INTRODUCTION

As a result of steady population increase, building energy consumption proportion of the world's energy use is expected to increase by 3% every year to 70% by 2050 (Mohammed et al, 2022). Major part of this energy consumption is used for building services of which about half of it is used for heating, ventilating and air conditioning the building envelopes (ASHRAE, 2005). With the aim of optimizing energy usage, researchers have conducted various studies and hence developed techniques that effectively control the components of building heating and cooling loads especially through the rooftops.

Effect of rooftop surface solar reflectivity on the heat gain by naturally ventilated and unventilated roofs was experimentally and numerically studied by Tong et al. (2014). Daily heat gain was found to increase by 11% for both types of roofs. A paraffin-based phase change material (PCM) was applied by Sinacka and Szczechowiak (2021) to a ceiling to determine the coefficient of heat transfer and the heat flux density. The results revealed that peak power occurred during the night that temperature would be lower thereby maintaining thermal comfort throughout the room occupied hours. Anna et al., (2023) numerically investigated natural convection in a pentagonal-shaped house under summer condition. Constant rate of heat flux was applied to the upper inclined surface of the roof, the cold surface maintained at constant temperature while the other parts were insulated.

*Corresponding Author

Section C- MECHANICAL/MECHATRONICS ENGINEERING & RELATED SCIENCES
Can be cited as:
Kamiyo O., and Dada A. (2024): Laminar Natural Convection in Attics of Rooftops with Depressed Walls, FUOYE Journal of Engineering and Technology (FUOYE**JET**), **9(2), 258-263.**
https://dx.doi.org/10.4314/fuoyejet.v9i2.15

It was observed that the variation of the mean Nusselt number on the hot wall with the Rayleigh number was strongly influenced by the heat flux. While testing the potentials of three different passive cooling roof techniques in residential buildings in hot arid regions, Athmani et al. (2023) monitored indoor and roof surface temperatures and found that thermal discomfort hours were reduced by 45% while the building cooling load was lowered by about 30%.

Aich, Hajri, & Omri (2011) numerically analysed natural convection in a prismatic roof and reported that increase in Rayleigh number and aspect ratio increased and decreased, respectively, the heat transfer from the heated bottom wall. Saha & Gu (2015) numerically investigated a case of uniform heating at the base wall of an isosceles triangular roof (depicting a pitched roof) when subjected to non-uniform cooling at the inclined walls. Three stages of flow development were observed. Heat transfer rate from the base wall was found to be unsteady after a critical Rayleigh number. Saleem & Alshara (2019) simulated a triangular roof with constant heat flux at the base wall while the inclined walls were exposed to external airstream cooling. They discovered that the heat transfer rate increased with the aspect ratio, Rayleigh number and cooling air freestream Reynolds number. Heat transfer rate across the walls of a 30° trapezoidal roof was studied by Mehryan et al. (2020). The results showed that heat transfer rate on the trapezoidal roof was 15% lower when compared to that in a square cavity. Cui et al., (2019) investigated unsteady natural convection in a sectioned triangular prismatic cavity heated from the basewall. The convective heat flux from the bottom wall was found to increase linearly with the aspect ratio and Rayleigh number.

Unlike many authors that worked on straight bottom walls, triangular roof having zig-zag base wall was

studied by Rahman et al. (2012) to show that, for the Rayleigh number range considered, the average rate of heat transfer increased with buoyancy ratio. Kamiyo (2020) also numerically simulated rooftops heated from a raised ceiling and noted that at low roof pitch, heat transfer rate was high and that it decreased as the aspect ratio increased.

In most cases, building aesthetics has been the focus in roof design while trading off thermal performance. Among such designs are pitched roofs with depressed upper side(s). This study analysed the airflow, thermal and heat transfer characteristics of pitched roofs with depressed upper walls. Three peculiar roof designs selected, viz, Butterfly, Clerestory and Combination, are compared with a standard triangular rooftop to effectively examine the impact of the depressed upper parts.

2 METHODOLOGY

Three common pitch roofs having different peculiar shapes with depressed upper surface selected for this study, with a standard isosceles triangular roof to be used as reference, are as shown in Fig. 1(a-d). The roofs are often referred to as Clerestory, Combination and Butterfly. The Clerestory is simply an isosceles triangle with a vertical wall truncating it at a location that varies in reality. Combination roof shape came out of two interwoven triangular cross-section with different angles. Butterfly roof has a cross-section of a standard isosceles triangle but with a fully inverted apex. The selected roofs are compared with the triangular roof to properly assess the effect of the depression. Two dimensional roof model is adopted to depict an attic with the length more than double the cross sectional width (Penot & N'Dame, 1992).

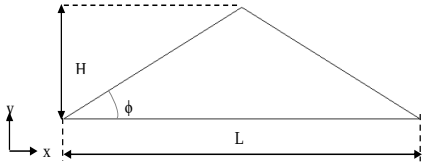

(a) Triangular

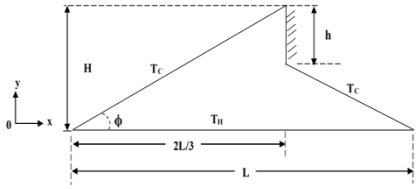

(b) Clerestory

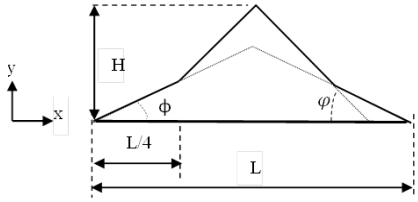

(c) Combination

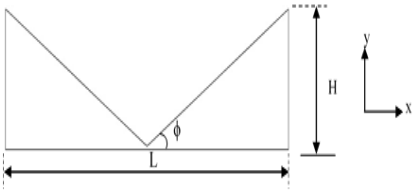

(d) Butterfly

Fig. 1. Physical models

Each roof is air-filled. The buoyancy-driven, steady, laminar natural convection flow in the attics, without heat generation, can be modelled using the following conservation equations:

Mass Conservation:

$$\frac{\partial U}{\partial X} + \frac{\partial V}{\partial Y} = 0 \quad (1)$$

Momentum Conservation:
U-momentum

$$U\frac{\partial U}{\partial X} + V\frac{\partial U}{\partial Y} = -\frac{\partial P}{\partial X} + Pr\left(\frac{\partial^2 U}{\partial X^2} + \frac{\partial^2 U}{\partial Y^2}\right) \quad (2)$$

V-momentum

$$U\frac{\partial V}{\partial X} + V\frac{\partial V}{\partial Y} = -\frac{\partial P}{\partial Y} + Pr\left(\frac{\partial^2 V}{\partial X^2} + \frac{\partial^2 V}{\partial Y^2}\right) + RaPr\theta \quad (3)$$

Energy Conservation:

$$U\frac{\partial \theta}{\partial X} + V\frac{\partial \theta}{\partial Y} = \left(\frac{\partial^2 \theta}{\partial X^2} + \frac{\partial^2 \theta}{\partial Y^2}\right) \quad (4)$$

where $X = \frac{x}{H}$; $Y = \frac{y}{H}$; $U = \frac{uH}{\alpha'}$; $V = \frac{vH}{\alpha'}$; $\theta = \frac{T-T_c}{T_H-T_C}$; $P = \frac{pH^2}{\rho\alpha'^2}$; $Ra = \frac{g\beta'\Delta T H^3}{\nu\alpha'}$; $Pr = \frac{\nu}{\alpha'}$

In reality, the roof pitch ϕ varies, but in this study, for ease of comparison, the pitch and the length of the base wall are the same for all the roofs. In all the cases, the physical domain coincides with the computational domain. The normalized boundary conditions are:

Temperature:

θ = 0 For cold inclined walls

θ = 1 For hot basewall

Velocity:

U=V= 0 No slip condition

Based on the geometry and boundary conditions, the Rayleigh number obtained for all the roofs is 1.59 x 10^7.

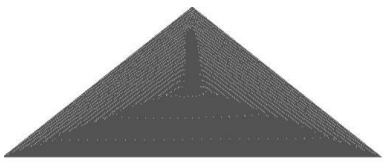

Fig. 2. Unstructured mesh for the Triangular roof

As shown in Fig.2 for the standard triangular roof, a fine mesh with unstructured tetrahedrons with high orthogonal quality was generated to discretize the computational domains. ANSYS FLUENT CFD package was employed for the simulation. Further details on the

https://dx.doi.org/10.4314/fuoyejet.v9i2.15 engineering.fuoye.edu.ng/journal

solution procedure is presented in Kamiyo & Ekundayo (2022).

Grid independence test was conducted by changing the number of elements for each roof shape. The maximum values of the relative velocity, U_{max}, for corresponding number of elements for the triangular roof is shown in Table 1. The table indicates that a mesh with 63,538 elements would be adequate to obtain results that do not depend on the grid generated.

Table 1. Grid test results for the Triangular roof

Number of elements	41,642	63,538	75,523
U_{max}	0.2200	0.2177	0.2178

The ability of ANSYS FLUENT to effectively and accurately stimulate the current laminar natural convection in roofs problem have been proved in the literature with similar configurations and solution approach (Saha & Gu, 2014; Yesiloz & Aydin, 2013). This thus validate the simulation technique adopted in this study.

3 RESULTS AND DISCUSSION

The results obtained are presented in Figs.3-10 in form of contour plots of the streamlines, temperature, velocity, pressure and graphical plots of the dimensionless temperature, velocity profile and the mean Nusselt number. The plots show clearly the influence of the depressed sections on the thermal and flow fields within the roofs.

3.1 STREAMLINES

Fig.3(a-d) show the patterns of airflow within the roofs. In a manner typical of roofs heated from the basewall, the streamlines in all the roofs displayed multiple counter-rotating cells formed by the convection system generated. As the basewall is heated, hot air rises, in form of plumes, through the attic towards the cold upper walls. On thrusting at an upper wall, a plume splits into two with each part flowing in either direction. Detaching from the upper wall, a jet of cold air flows back to the basewall. The cycle repeats to form a pattern of cells of different sizes rotating in opposing directions and at varying speeds. A jet to the right of a plume implies the cell rotates clockwise while the cell rotates counterclockwise when the jet is to the left. The size and rotating speed of a cell reduce from the wider area of a roof towards the bottom corners.

(a) Triangular

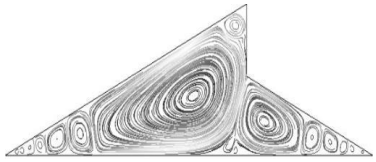

(b) Clerestory

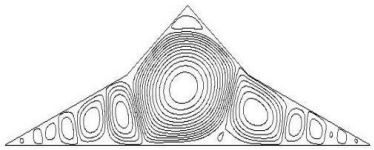

(c) Combination

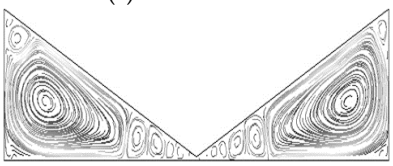

(d) Butterfly

Fig. 3. Streamlines of the airflow

In the Triangular roof, Fig.3a, thirteen cells are formed. A large cell occupies the wide middle area. The size and rotating speed of other cells on either side of it reduce towards the corners. In the other roofs however, the shape of the roof strongly impact on the number and size of the cells formed. Clerestory roof in Fig.3b has a depressed part that divides the roof into two sections. The vertical wall, which could be on either side of the roof and at any point along the length, caused the formation of different flow patterns on each half of the roof. On the left, a large, elongated vortex occupying about two-third of the half dominates the flow system there. Towards the corner of the left half, few and weak counter-rotating cells are formed. On the right half, the closeness of the upper and lower walls results in further breakdown of the cells and reduction in their sizes and rotating speeds. A plume rising from the basewall below the vertical wall hits the bend and bifurcates to form the big cell rotating clockwise on the right half and the larger cell on the left half rotating anticlockwise. A small clockwise rotating cell is formed at the sharp apex mainly due to the fluid separated from the large cell and entrapped within the corner.

In the Combination roof, depression of the upper walls created a large space at the middle occupied by a large cell. The depression brings the upper walls closer to the basewall thereby causing further breakdown of the cells. Eleven of the twelve cells in the roof fall under the depressed walls. Being reversed shapes, the airflow patterns in the left and right halves of the standard Triangular roof (Fig.3(a)) are respectively similar to that within the right and left of the Butterfly roof. As in the case of the Clerestory roof, a small cell is formed at the sharp apex of each half of the Butterfly roof.

3.2 TEMPERATURE DISTRIBUTION

https://dx.doi.org/10.4314/fuoyejet.v9i2.15 engineering.fuoye.edu.ng/journal

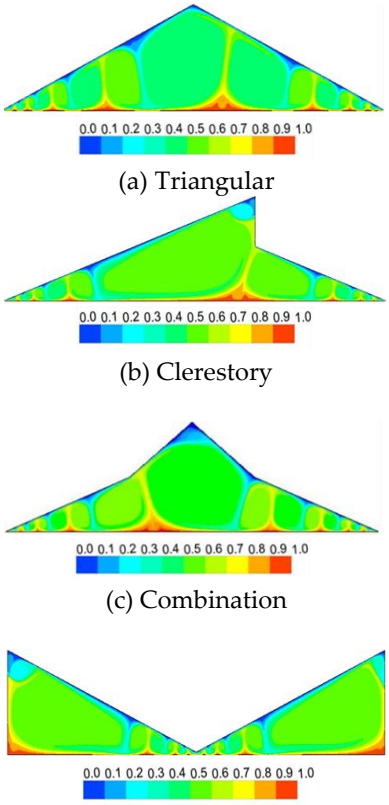

(a) Triangular

(b) Clerestory

(c) Combination

(d) Butterfly

Fig. 4. Temperature distribution

In all the roofs, hot air rising as plumes from the basewall appear like mangrove trees while cold jets dropping down from the upper walls are like inverted trees. In between a plume and an adjacent jet, a cell is formed. In Fig. 4(a), there are seven plumes and seven jets indicating fourteen cells (shown in Fig 3(a)). The symmetry shape of the Triangular roof results in fairly non-uniform temperature distribution with small conduction region at the corners. The two large cells at the middle of the roof have average temperature of about θ=0.4. But towards the bottom corners, the temperature increased to about θ=0.5. About one-third of the roof volume at the middle is at a lower temperature than within the other one-third on either side. This is understandably due to the reducing volume of cold air to be heated as the walls get closer.

In Fig.4(b) for the Clerestory roof, there are five plumes and five jets each pair enclosing a cell. Temperature is fairly uniform at θ=0.5 across it except at the peak where the temperature is about θ=0.2. The Combination roof in Fig.4(c) also showed a non-uniform temperature distribution. The large cell between the bends has an average temperature of θ=0.4. Between the bend and the bottom corner of each half, the temperature is averagely θ=0.6 especially around the plumes. The depression of the upper walls therefore increases the temperature within the roof. Fig.4(d) indicates generally uniform temperature distribution of θ=0.5 within the butterfly roof. There are four plumes and three jets in each half. Plumes rising along the vertical walls on either side require that the vertical walls be made of heat resistant materials.

3.3 VELOCITY DISTRIBUTION

In Fig. 5, the predicted results for the air velocity variation within the roofs are shown. The patterns generally indicate that as hot air rises from the base wall as a plume, air velocity increases, gets to a peak and then reduces as the plume loses momentum while pushing though the cold dense air before hitting the upper wall. Flowing down the inclined wall under gravity, the air velocity increases till it detaches at the base of a jet and flows downward. The air velocity profile along the path of a plume from the basewall to the inclined wall is similar to that along the path of a jet from the upper wall to the base wall. In all the roofs, air convection reduces as the walls converge. In the Clerestory roof, the depressed wall damps the rotation of the cells. Similar effect is observed after the bends in the Combination roof. In the Butterfly roof where the apex is inverted, there is a reverse in the cell arrangement, size and rotational speed in comparison with that of the Triangular roof.

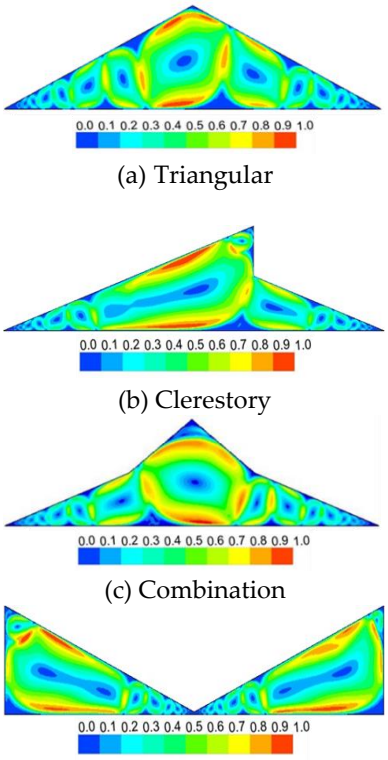

(a) Triangular

(b) Clerestory

(c) Combination

(d) Butterfly

Fig. 5. Air velocity distribution

3.4 PRESSURE DISTRIBUTION

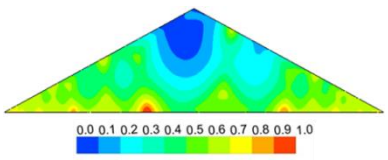

(a) Triangular

https://dx.doi.org/10.4314/fuoyejet.v9i2.15 engineering.fuoye.edu.ng/journal

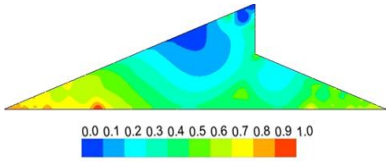

(b) Clerestory

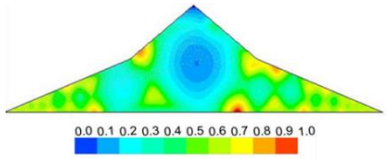

(c) Combination

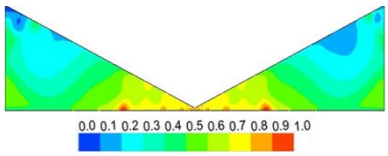

(d) Butterfly

Fig. 6. Air pressure patterns

Fig. 6(a) indicates that near the apex of the Triangular roof, air pressure is very low (P<0.2) as air movement along the rotating cell is high. It increased uniformly outward to about P=0.4. Within a region covering a third of the length of the basewall from each corner of the roof, pressure ranges between P=0.5 and P=0.6. In the Clerestory roof, Fig. 6(b), the pattern is similar except that the pressure is higher at the left bottom corner (0.6<P<0.8). The Combination roof shows pressure increasing outwardly from the core of the central cell inversely to the velocity variation at the roof's midsection. Between the bends and the bottom corners, pressure is high at the base and tip of the jets and plumes (0.3<P<0.7). In Fig. 6(d), Butterfly roof has the highest pressure at the depressed centre within the range of P=0.6 and P=0.9. It reduces towards the vertical wall in both halves.

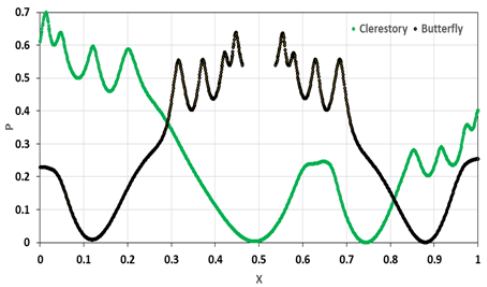

Fig. 7. Pressure across height Y= 0.1H in the Clerestory and Butterfly roofs

To know the pressure objects placed on the ceiling would be subjected to under the applied boundary conditions, pressure values at the height Y=0.1H was plotted and presented in Fig. 7 for the Clerestory and Butterfly roofs. Variation of pressure across the basewall span of the Clerestory roof shows that, on the left side, pressure reduces from the bottom corner to the middle. But on the right side, the depressed wall acted as a damper, decreasing the pressure within the area to about half of that on the left side. In the Butterfly roof, pressure is low along the outer edge of the large elliptical cell where the air speed is relatively high. It increases in sequence with the arrangement of the slow moving cells towards the middle of the roof. A good balance between effects of air pressure and airspeed is required for object placement within the attic.

3.4 HEAT TRANSFER

Minimizing the heat flow across the ceiling which determines the thermal performance of the roof has been the main goal of rooftops designers. The rate of heat transfer between hot and cold walls of the roof has been found to depend on the distance between them. This heat rate can be determined by the variation of either local heat transfer coefficient or local surface heat flux across the hot ceiling. The overall rate of heat flow into the attic is determined by the average Nusselt number of the hot base wall in the roofs. According to Bejan (2013), the average Nusselt number is defined as

$$\overline{Nu} = \frac{\bar{q}\,L}{k_f\,\Delta T} \quad (5)$$

where L, the length of the basewall, is same for all the roofs.

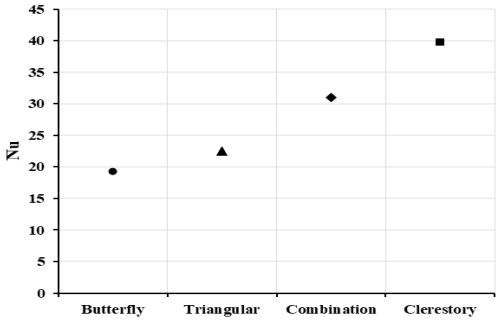

Fig. 8. Mean Nusselt number for the hot basewalls

In Fig. 8, the Butterfly roof is having the lowest value of $\overline{Nu}$ because heat convection is only high at the midsection of the basewall which is just about one-third of the length. $\overline{Nu}$ is higher in the Combination and Clerestory roofs than in the Triangular roof because of the depressed wall that brings the hot and cold walls closer and hence, increase the heat exchange between them.

4 CONCLUSION

Laminar natural convection in roofs with depressed upper walls has been investigated numerically using ANSYS FLUENT package. Selected roofs referred to as Combination, Clerestory and Butterfly are compared with isosceles Triangular roof with the same pitch and base length. The results obtained show that the depressed wall distorts the multicellular air movement pattern within the attics. It compressed the cells, thereby reducing their sizes and damping their rotation. In the Combination roof in particular, the depressions bring the

https://dx.doi.org/10.4314/fuoyejet.v9i2.15 engineering.fuoye.edu.ng/journal

upper walls closer to the base wall causing further breakdown of the cells and redistribution of velocity and temperature fields. Air pressure is higher under the depressed wall than other areas within the attic. Heat transfer rate also increased under the area covered by the depressed wall. Overall, the mean heat transfer rate is found to increase with the depth and length of the depressed wall. It is therefore concluded that the depression in the roofs influence the flow field, the thermal field, heat flow patterns within the roofs and increase the rate of heat loss across the ceiling.

NOMENCLATURE

g	Acceleration due to gravity, m/s²
H	Height of roof, m
L	Length of roof, m
Pr	Prandtl number
p	Air pressure, N/m²
P	Dimensionless pressure
$\bar{q}$	Mean surface heat flux
Ra	Rayleigh number
T	Air temperature, K
T_C	Inclined walls temperature, K
T_H	Base wall temperature, K
u	Air velocity in x-axis, m/s
U, V	Dimensionless velocity
v	Air velocity in y-axis, m/s
x, y	Cartesian coordinates
X, Y	Dimensionless Cartesian coordinates

Greek symbols

α'	Thermal diffusivity, m²/s
β'	Coefficient of thermal expansion, K^{-1}
θ	Dimensionless temperature
ν	Kinematic viscosity, m²/s
ϱ	Density, kg/m³

REFERENCES

Aich, W., Hajri, I., & Omri, A. (2011). Numerical analysis of natural convection in a prismatic roof. *Thermal Science*, *15*(2), 437-446. doi.org/10.2298/TSCI1102437A

ASHRAE (2005). Load and Energy Calculations *ASHRAE Handbook - Fundamentals* (ch.28): ASHRAE.

Athmani, W., Sriti, L., Dabaieh, M., & Younsi, Z. (2023). The potential of using passive cooling roof techniques to improve thermal performance and energy efficiency of residential buildings in hot arid regions, *Buildings, 13*(1), 21-44. doi.org/10.3390/buildings13010021

Bejan, A. (2013). Laminar Boundary Layer Flow *Convection Heat Transfer*, 4th edition (pp.55): John Wiley & Sons.

Cui, H., Xu, F., Sahad, S., & Liu, Q. (2019). Transient free convection heat transfer in a section triangular prismatic roof with different aspect ratios, *International Journal of Thermal Sciences*, *139*, 282-291. doi.org/10.1016/j.ijthermalsci.2019.02.023

Kamiyo, O. (2020). Numerical simulation of natural convection for raised-ceiling rooftop heated from below. *Kufa Journal of Engineering*, *11*(4), 58-71. doi.org/10.30572/2018/KJE/110405

Kamiyo, O., & Ekundayo, O.E. (2022). Comparative thermal performance analysis of rooftops with elevated ceiling configuration. *Kufa Journal of Engineering*, *13*(4), 39-52. doi.org/10.30572/2018/KJE/130404

Li, A., Wang, T., Xi, G., & Huang, Z. (2023). Laminar natural convection in a 2-D pentagonal house with sloping roof heated by constant heat flux. *Numerical Heat Transfer, Part A: Applications, 83*(4), 361-378. doi: 10.1080/10407782.2022.2091383

Mehryan, S.M., Mohammad, G., Reza, K.F., Ahmad, H., & Mohsen, I. (2020). Free convection in a trapezoidal roof divided by a flexible partition, *International Journal of Heat and Mass Transfer*, *149*(119186), 14 pages. doi.org/10.1016/j.ijheatmasstransfer.2019.119186

Mohammed, A., Tariq, M. A. U. R., Ng, A. W. M., Zaheer, Z., Sadeq, S., Mohammed, M., & Mehdizadeh-Rad, H. (2022). Reducing the cooling loads of buildings using shading devices: a case study in Darwin. *Sustainability*, *14*(7), 3775-3795 doi 10.3390/su14073775

Penot, F., & N'Dame, A. (1992). Successive bifurcations of natural convection in a vertical roof heated from the side', Heat Transfer. *3rd UK National Conference and First European Conference on Thermal Sciences*, *1*, 507-513.

Rahman, M., Oztop, H., Ahsan, A., & Orfi, J., (2012). Natural convection effects on heat and mass transfer in a curvilinear triangular cavity. *International Journal of Heat and Mass Transfer 55*, 6250–6259. doi:10.1016/j.ijheatmasstransfer.2012.06.055

Saha, S., & Gu, Y. (2014). Transient air flow and heat transfer in a triangular roof with a conducting partition. *Applied Mathematical Modelling, 38,* 3879-3887. doi.org/10.1016/j.apm.2013.10.006

Saha, S., & Gu, Y., (2015). Natural convection in a triangular roof heated from below and non-uniformly cooled from top. *International Journal of Heat and Mass Transfer*, *80*, 529–538. doi.org/10.1016/j.ijheatmasstransfer.2014.09.047

Saleem, K., & Alshara, A., (2019). Natural convection in a triangular cavity filled with air under the effect of external air stream cooling, *Heat Transfer*, *48*(7), 3186-3213. doi.org/10.1002/htj.21537.

Sinacka, J. & Szczechowiak, E., (2021), An experimental study of a thermally activated ceiling containing phase change material for different cooling load profiles. *Energies*, *14*, 7363. doi.org/10.3390/en14217363.

Tong, S., Li, H., Zingre, K., Wan, M., Chang, W., Wong, S., Toh, W., & Lee, I. (2014). Thermal performance of concrete-based roofs in tropical climate. *Energy and Building*, *76*, 392–401. doi.org/10.1016/j.enbuild.2014.02.076

Yesiloz, G. & Aydin, O. (2011). Natural convection in an inclined quadrantal cavity heated and cooled on adjacent walls. *Experimental Thermal and Fluid Science*, *35*, 1169–1176. doi.org/10.1115/1.4003044